

© 2021 IEEE. Personal use of this material is permitted. Permission from IEEE must be obtained for all other uses, in any current or future media, including reprinting/republishing this material for advertising or promotional purposes, creating new collective works, for resale or redistribution to servers or lists, or reuse of any copyrighted component of this work in other works.

Digital Object Identifier 10.1109/TTE.2021.3059790

IEEE Transactions on Transactions on Transportation Electrification

Voltage-Dependent Load Levelling Approach by means of Electric Vehicle Fast Charging Stations

Xiang Gao
Giovanni De Carne
Markus Andresen
Sebastian Brüske
Sante Pugliese
Marco Liserre

Suggested Citation

X. Gao, G. De Carne, M. Andresen, S. Brüske, S. Pugliese and M. Liserre, "Voltage-Dependent Load Levelling Approach by means of Electric Vehicle Fast Charging Stations," in *IEEE Transactions on Transportation Electrification*.

Voltage-Dependent Load Levelling Approach by means of Electric Vehicle Fast Charging Stations

Abstract—Intermittent generation and load demand are one of the major challenges for grid operators. Caused for example by renewables power variability or electric vehicle charging, it can create mismatches between the realtime and forecasted demand, affecting frequency regulation. To alleviate this mismatch, operators have to resort either on the balancing market or on extensive use of energy storage systems, which increases operation costs. This paper introduces a load levelling approach exploiting the voltage dependency of the loads. With a controlled reactive power injection, the converters of fast charging stations can influence the voltage profile, and consequently the power consumption of voltage-dependent loads. The approach has two main goals: minimizing the mismatches with respect to the demand forecast and reducing the grid losses. Fast charging stations are particularly suited for this approach. Being employed with full capacity for charging only for short-time, their spare capacity can be exploited to apply the load levelling approach. This proposed approach is discussed theoretically and analyzed in a modified distribution network in Northern Germany. Parameters variation analysis has been performed to thoroughly demonstrate the effectiveness of the approach under different load/grid conditions. Its feasibility has been evaluated by means of power-hardware-in-the-loop tests.

Index Terms—Fast charging station, load levelling, losses minimization, power-voltage sensitivity, reactive power control.

I. INTRODUCTION

THE increasing integration of renewable energy sources (RES) and the electrification of the transportation sector are transforming the electrical system. From scheduled production and easily foreseeable demand, it is moving towards intermittent production, depending on the natural resource availability (e.g. solar irradiation) and non-predictable demand (e.g. customer-dependent charging of the electric vehicles). As a consequence, the net-load demand (load minus generation from RES) becomes strongly variable and not easily predictable [1]. Of particular concern for operators, large power mismatch between realtime demand and the demand forecast can cause large frequency deviations, endangering the system stability.

To mitigate the power mismatch, energy storage systems (ESS) are being installed, acting as primary energy reserves. In the literature, several ESS-based methods have been proposed to mitigate the demand volatility. A dual-layer control strategy has been proposed, which consists of a fluctuation mitigation layer and a power allocation layer [2]. The control schemes of renewable power/ESS hybrid systems have been analyzed, which are used to smooth the power generation of different intermittent sources [3], [4]. A concurrent redispatch scheme has been proposed to help a distribution grid track the dispatch plan and its performance has been assessed with field tests [5]. Despite all the aforementioned ESS-based methods have been

proven to effectively mitigate the demand mismatch, it is well-known that the deployment of the ESS increases system costs (initial investment plus maintenance). As a consequence, the installation of ESS must be limited to some strategic points in the grid. In addition, repetitive power cycling can affect the lifetime of commonly used storage technologies, such as batteries [6], suggesting rapid reduction of cycling operations.

As an alternative to the energy storage for mitigating the demand mismatch, the load power consumption can be exploited. By adjusting the demand of controllable loads (e.g. heat, ventilation, and air conditioning systems), the forecast load baseline can be tracked [7]. Using aggregated deferrable loads has been proved effective to control the demand [8]. Electric vehicles (EVs) have also been exploited as controllable loads, offering services such as congestion management, primary frequency control, and RES integration services [9]–[15]. However, the demand response methods have two main drawbacks. Firstly, it requires an extensive communication infrastructure, in order to estimate the grid status. Secondly, it requires the permission of customers for participating into the service. Furthermore, their performance can be affected by the customer's will to modify existing daily patterns, e.g. charging the EV during the night instead in the day.

To compensate the limitations of ESS-based and demand response-based solutions, this paper introduces a load levelling approach, implemented by fast charging stations (FCSs). The approach regulates the voltage profile in the medium voltage (MV) grid by means of controlled reactive power injection from the FCSs. The novelty of this approach lies in the exploitation of the voltage-dependent load's characteristic to vary the power consumption by regulating the voltage magnitude. This offers the possibility to shape the load demand without the need of additional hardware such as batteries. FCS is the perfect candidate as actuator due to its aggregated high power rating and limited full utilization over time. While the FCS meets the charging power demand of any connected EVs, its converters can use the large spare capability for reactive power injection. This approach makes fully use of the FCSs to provide grid control service, benefiting the grid operation especially under high penetration of FCSs.

The paper is structured as follows: Section II introduces the basic principle and actuators for the proposed approach. Section III describes the algorithm to implement the approach. Section IV presents the MV network used as benchmark and the investigated scenarios, while Section V depicts the obtained results and analyzes the performance of the proposed approach in steady state. The results of power-hardware-in-the-loop (PHIL) tests, which demonstrates the practicality and feasibility of this approach with hardware, are presented in section VI. Finally, the conclusions are drawn in Section VII.

TABLE I
PARAMETERS OF THE SIMPLIFIED FEEDER SHOWN IN FIG. 3

Case No.	R/X ratio	Z (p.u.)	SCC (p.u.)	P_{load} (p.u.)	Power factor
1	4/3	0.005	10	2	1
2	4/3	0.005	20	2	1
3	4/3	0.005	50	2	1

optimization of the grid. All measurements are collected by the control center, as shown in Fig. 2. Measurement $\text{Load}_y(t)$ of each controlled bus y , which contains the power-voltage sensitivity $k_{py}(t)$, $k_{qy}(t)$, voltage $V'_{\text{load}y}(t)$, and load demand $P'_{\text{load}y}(t)$, $Q'_{\text{load}y}(t)$ of this bus (here the prime sign on symbols implies without load levelling), is sent to the control center. It receives also the tap position of the on-load tap changer (OLTC) used as further support actuator for the load levelling. The grid demand forecast profile $P^*_{\text{grid}}(t)$ is derived based on historical data. However, a mismatch between the forecast and realtime power demand may occur. The role of the control center is to determine the needed reactive power injection $Q_{\text{FCS}x}(t)$ ($x = 1, 2, \dots, m$) of FCS x , based on the measured and forecasted power demand. As shown in Fig. 1 (a), all FCSs involved in the approach inject reactive power according to setpoints formulated by the control center, which regulates the voltage of each bus from $V'_{\text{load}y}(t)$ to $V''_{\text{load}y}(t)$ (double prime sign represents with load levelling) as shown in Fig. 1 (b). Accordingly to the power-voltage sensitivity, each load varies its power consumption $P''_{\text{load},y}(t)$ following the new voltage profile $V''_{\text{load}y}(t)$ (Fig. 1 (c)). The power of the entire grid $P''_{\text{grid}}(t)$, i.e. the power of the HV/MV substation, is controlled to track the grid forecast power $P^*_{\text{grid}}(t)$ with a reduced mismatch, as shown in Fig. 1 (d).

The charging power supply to the EVs is the first priority for the load levelling approach. As mentioned in the introduction, it exploits only the spare capacity of FCS to inject reactive power into the grid, without affecting the active power demand of the EVs. As a consequence, the EV batteries state of charge are not affected by the proposed approach [22].

C. Performance analysis under different grid conditions

To evaluate the effectiveness in controlling the power consumption of voltage-dependent load by means of reactive power, the feeder shown in Fig. 3 (a) is used under different short circuit capacity (SCC). The analysis has been carried out assuming that the feeder R/X ratio is equal to 4/3, and each grid impedance is equal to $Z_{\text{grid}} = Z_{\text{load}} = Z_{\text{FCS}} = 0.005$ p.u. The base values of voltage and power are 11 kV and 1 MVA, respectively. All parameters are summarized in Table I. To simplify this initial analysis, without lacking in generality, it has been assumed that the FCS does not absorb any active power, injecting only reactive power.

Figs 3 (b)-(d) show the impact on the power consumption P_{load} from the FCS reactive power injection under different sensitivity coefficients. As can be noted in Fig. 3 (b), in the case of a weak grid (SCC= 10 p.u.) and constant impedance

load, an active power variation up to 4 % can be achieved with limited (0.2 p.u.) reactive power injection. If a higher SCC is considered (SCC= 20 p.u.), the control margin is reduced to about 2 % power variation, as shown in Fig. 3 (c). Although the impact on the power variation is lower than the previous case, a 2 % power control can still offer load levelling services to the grid. However, as shown in Fig. 3 (d), with an SCC of 50 p.u., the power deviation can reach at maximum 1 %, also under high reactive power injection. In the case of a strong grid, more FCSs have to be considered for providing higher power controllability.

D. OLTC-based conservation voltage reduction

The CVR represents a well-known example to use the transformers' OLTC as actuator in varying the consumption of voltage-dependent loads, by adjusting the OLTC ratio within the operator's defined permissible range [23], [24]. Having been tested in different countries such as USA, Australia, and Ireland, the CVR has proven effective in different load control applications [23]. Its only hard constraint is to respect the voltage safe limits (e.g., $\pm 10\%$ of the nominal voltage) in the whole grid. However, in comparison with the FCSs based load levelling approach, the CVR can offer only slow control actions due to the limited mechanical switching frequency, which affects the dynamic behavior. Furthermore, frequent operation of OLTC results in fast mechanical wear, reducing significantly the lifetime of the tap-changer.

In this paper, the use of CVR has been included within the load levelling approach, considering the tap change position of any value within the interval:

$$t_{\text{OLTC}}(t) \in [t_{\text{OLTC,min}}, t_{\text{OLTC,max}}] \quad (3)$$

where $t_{\text{OLTC}}(t)$ is the current tap position of OLTC, $t_{\text{OLTC,min}}$ and $t_{\text{OLTC,max}}$ are the lowest and highest position of the OLTC, respectively. $t_{\text{OLTC}} = 0$ means that the voltage conversion rate of the transformer is 1:1 p.u.

The overall timeline to implement the proposed load levelling approach is presented in Fig. 4. The power-voltage sensitivity is periodically estimated. After the activation of the load levelling approach, it takes approximately 10-15 s to set the new reactive power setpoints of FCSs. This delay takes into account the measurement communication delay, the execution time of the algorithm in the control center, and the transmission of the new setpoint to each FCS. A communication delay in the order of seconds has been estimated in this case, considering a communication infrastructure based on industrial protocols such as ModBus, which typically has a communication delay of about 0.5-1 s. The signal to activate the OLTC for load levelling is held by the control center at least one minute after the FCSs have adjusted the new reactive power setpoints. Then, if the detected power mismatch is still higher than a threshold value, the control center sends an action signal to the OLTC. Since the sensitivity of the aggregated load changes much slower than the approach implementation, the update of sensitivity is considerably much less frequent than the implementation of the proposed approach.

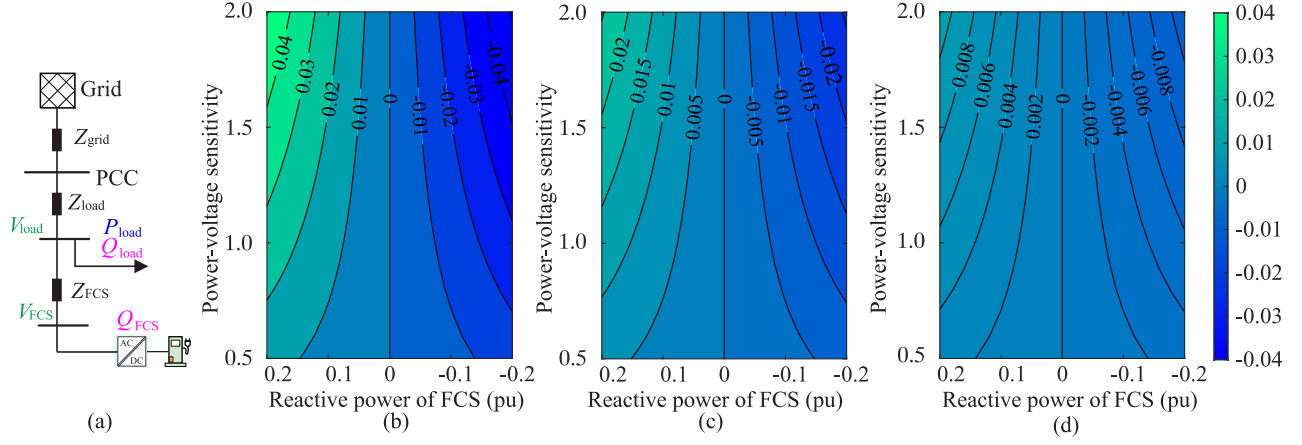


Fig. 3. Change of power consumption with different reactive power injection and power-voltage sensitivity in a simplified MV feeder. (a) Structure of simplified feeder. (b) SCC of Grid 10 p.u. (c) SCC of Grid 20 p.u. (d) SCC of Grid 50 p.u.

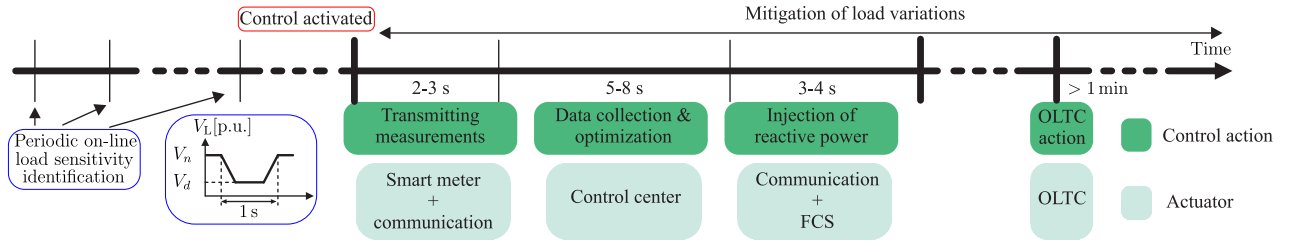


Fig. 4. Timeline for the actions and the related actuators of the proposed load levelling approach.

III. OPTIMIZATION ALGORITHM OF CENTRALIZED LOAD LEVELLING APPROACH

This section gives a detailed description of the implementation algorithm for the voltage-dependent load levelling approach.

In order to determine the actuators' setpoints, a multi-objective optimization algorithm is formulated. Every scheduled time (e.g. 15 minutes), based on the grid demand forecast $P_{grid}^*(t)$, the collected measurements including the power, voltage, and load sensitivity coefficients from every bus of the grid, the control center computes the new reactive power setpoints of FCSs and the new OLTC position by means of a nonlinear programming based optimization to mitigate the power mismatch of $P_{grid}(t)$ in relation to the forecast $P_{grid}^*(t)$. The optimization is implemented with the software GAMS (General Algebraic Modeling System). It is a high-level modeling software for mathematical optimization with solvers for different linear, nonlinear, and mixed-integer optimization problems.

The approach includes a two-stage optimization, as described in Fig. 5. Stage 1 computes the setpoints of the FCSs' reactive power injection and the tap position of the OLTC, targeting a minimization of the power mismatch ($|P_{grid}(t) - P_{grid}^*(t)|$). If the mismatch is completely mitigated, stage 2 adjusts the reactive power injection of all FCSs to minimize the total power transfer losses of the grid. In stage 1, multipole local minima can occur. In stage 2, the objective is to identify the minimum, in which the minimum losses in

the grid can be achieved. The description of the two stages of the optimization algorithm are described below.

A. Stage 1: mitigation of demand power mismatch

As mentioned above, the objective of stage 1 is the load levelling. The objective function is to minimize the difference between measured and forecast active power demand:

$$F_1 = \min(|P_{grid}(t) - P_{grid}^*(t)|) \quad (4)$$

subject to:

$$\begin{aligned} -P_{loadk}(t) &= V_k(t) \sum_{j=1}^{N_B} V_j(t) [G_{kj} \cos(\delta_k(t) - \delta_j(t)) + \\ &\quad B_{kj} \sin(\delta_k(t) - \delta_j(t))] \\ -Q_{loadk}(t) &= V_k(t) \sum_{j=1}^{N_B} V_j(t) [G_{kj} \sin(\delta_k(t) - \delta_j(t)) - \\ &\quad B_{kj} \cos(\delta_k(t) - \delta_j(t))] \end{aligned} \quad (5)$$

$$\begin{aligned} P_{loadk}(t) &= P_{loadk0} (V_k(t)/V_{k0})^{k_{pk}(t)} \\ Q_{loadk}(t) &= Q_{loadk0} (V_k(t)/V_{k0})^{k_{qk}(t)} \end{aligned} \quad (6)$$

$$V_{min} \leq V_k(t) \leq V_{max} \quad k = 1 \dots N_B \quad (7)$$

$$Q_{FCSx}^2(t) \leq S_{FCSx}^2 - P_{FCSx}^2(t) \quad x = 1 \dots m \quad (8)$$

$$\cos \varphi_{sub,min} \leq \cos \varphi_{sub}(t) \quad (9)$$

$$t_{OLTC,min} \leq t_{OLTC}(t) \leq t_{OLTC,max} \quad (10)$$

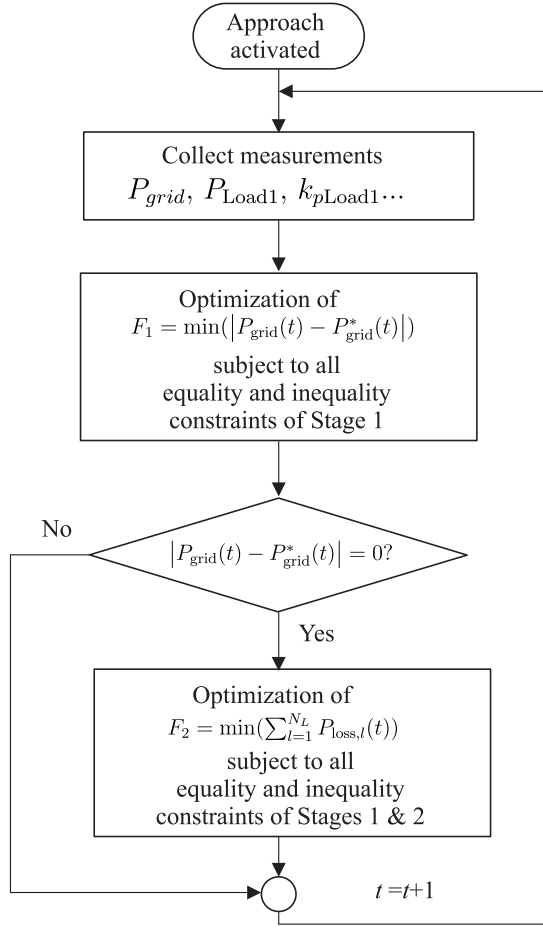


Fig. 5. Flow chart for implementation of the two-stage optimization. F_1 : mitigation of demand power mismatch. F_2 : minimization of losses.

$$\begin{cases} t_{\text{OLTC}}(t) - 1 \leq t_{\text{OLTC}}(t+1) \leq t_{\text{OLTC}}(t) + 1 & a = 0 \\ t_{\text{OLTC}}^*(t) - 1 \leq t_{\text{OLTC}}(t) \leq t_{\text{OLTC}}^*(t) + 1 & a = 1 \end{cases} \quad (11)$$

$$\begin{cases} V_{\text{OLTC}}^* - \epsilon \leq V_{\text{OLTC}}(t) \leq V_{\text{OLTC}}^* + \epsilon & a = 0 \\ V_{\min} \leq V_{\text{OLTC}}(t) \leq V_{\max} & a = 1 \end{cases} \quad (12)$$

where the grid buses, including FCSs, loads, and substation are $N_B = m + n + 1$, $P_{\text{load}k}(t)$ and $Q_{\text{load}k}(t)$ are the active and reactive power of bus k ($k = 1 \dots N_B$), $\delta(t)$ is the bus angle; G_{kj} and B_{kj} are the conductance and susceptance of the admittance matrix Y_{kj} between bus k and bus j , V_{\min} and V_{\max} are the voltage limits, $Q_{\text{FCS}x}(t)$ is the reactive power injection, and $S_{\text{FCS}x}$ and $P_{\text{FCS}x}(t)$ are the power rating and charging power of FCS at bus x , $\cos\varphi_{\text{sub}}(t)$ is the power factor of the substation, t_{OLTC} is the position of the OLTC and a is the binary trigger signal for the OLTC, $t_{\text{OLTC}}(t)$ is the position of OLTC at t , t_{OLTC}^* is the position which is derived by the local OLTC controller, V_{OLTC} and V_{OLTC}^* are the measurement and setpoint of the OLTC bus voltage, and ϵ represents the voltage deadband of the local OLTC controller.

The restriction of the OLTC actions at the HV/MV substation must be imposed. In the approach, the OLTC is activated, i.e. trigger signal $a = 1$, only if the following criteria are met:

- no voltage in the grid exceeding $[V_{\min}, V_{\max}]$.

- a minimal time interval of 15 min has occurred before the last load levelling action with OLTC.
- the power mismatch is higher than 8 % with respect to the grid forecast.

B. Stage 2: minimization of losses

If stage 1 is able to fully mitigate the power mismatch, stage 2 is activated to optimize the reactive power output of FCSs. The optimization function becomes:

$$F_2 = \min\left(\sum_{l=1}^{N_L} P_{\text{loss},l}(t)\right) \quad (13)$$

where:

$$P_{\text{loss},l}(t) = R_{kj} \cdot \frac{P_{kj}^2(t) + Q_{kj}^2(t)}{V_k^2(t)} \quad (14)$$

$$\begin{aligned} P_{kj}(t) &= V_k^2(t)G_{kj} - V_k(t)V_j(t)[G_{kj}\cos(\delta_k(t) - \delta_j(t)) + B_{kj}\sin(\delta_k(t) - \delta_j(t))] \\ Q_{kj}(t) &= V_k^2(t)G_{kj} - V_k(t)V_j(t)[G_{kj}\sin(\delta_k(t) - \delta_j(t)) - B_{kj}\cos(\delta_k(t) - \delta_j(t))] \end{aligned} \quad (15)$$

$P_{\text{loss},l}(t)$ are the losses on line l , N_L is the number of lines in the grid, R_{kj} is the resistance of the line l impedance $Z_{kj} = 1/Y_{kj}$ between the buses k and j .

The optimization problem remains subject to the same constraints (5)-(12), with the addition of the further power equality constraint:

$$|P_{\text{grid}}(t) - P_{\text{grid}}^*(t)| = 0 \quad (16)$$

IV. NETWORK UNDER STUDY AND TESTING CASES

In order to evaluate the performance of the proposed load levelling approach, an MV network is modeled in GAMS, following the indication of a local distribution system operator in Northern Germany. Different scenarios and cases are designed for the evaluation. The evaluation is implemented with a base voltage of 11 kV and a base power of 1 MVA.

A. Network under study and scenarios of analysis

The topology of the network under study is shown in Fig. 6. The HV/MV substation is equipped with an 11-position OLTC, covering a voltage range between 0.95–1.05 p.u. The original position of the OLTC is 0, i.e. 1 p.u. The MV network is composed of eight feeders with different lengths (from 3 km to 10 km) and 75 buses. The data of network is suggested by the German system operator. In every feeder, one FCS is assumed. The idea for only one FCS per feeder is similar to the petrol stations concept. As there is normally one (or few) petrol station per small urban district, there will be one FCS for each electrical feeder. The power rating of FCS is 0.60 p.u.

Fig. 7 (a) shows the 24h demand forecast profiles for single residential or commercial loads and single FCS. The base power $P_{\text{load}0} + jQ_{\text{load}0}$, which is depicted as 100 % in Fig. 7 (a), is $(0.35+j0.05)$ p.u. of the residential load and $(0.36+j0.09)$ p.u. of the commercial one, respectively. The 24h demand forecast profile of FCS (base power 0.60 p.u.) is

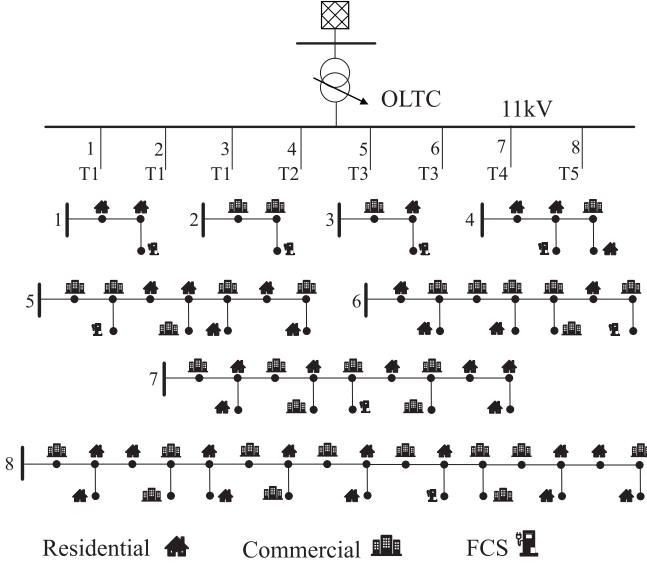


Fig. 6. Structure of testing network with 8 feeders at 11 kV.

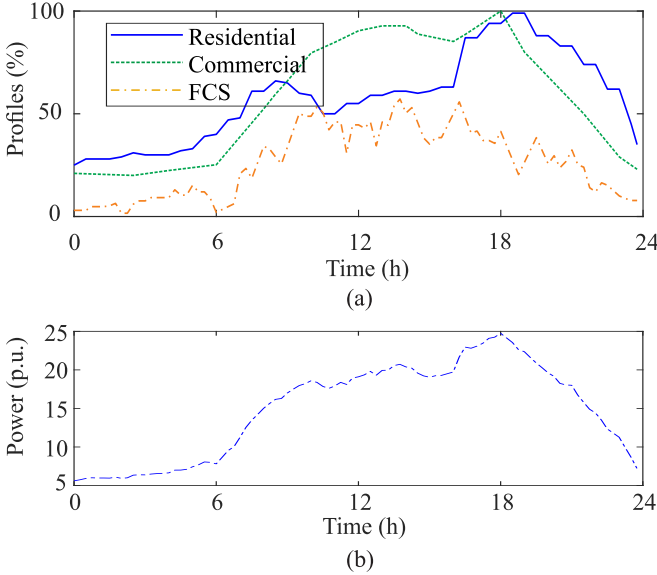


Fig. 7. 24 h power profiles. (a) Profiles of single residential or commercial load and single FCS. (b) Grid demand forecast profile.

presented in Fig. 7 (a). It is well-known that predicting the EV charging profile is extremely important for load management [25]. The forecasting methods can refer to previous researches such as [26]–[28]. The grid demand forecast, seen from the HV/MV substation, is the summary of power demand of all loads, FCSs together with the losses, which has a peak active power demand of approximately 25 p.u., as shown in Fig. 7 (b).

The realtime load or FCS consumption does not perfectly follow the forecast due to the variable consumption patterns of the users, resulting in the power mismatch in relation to forecast profiles in Fig. 7 (a). Previous works have demonstrated that the deviations from forecast profile can be presented by Gaussian distribution. The derived profiles in Fig. 7 (a) can represent the mean profiles. The variation of realtime

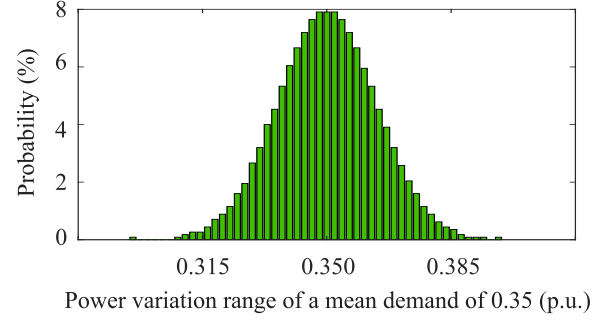


Fig. 8. Probability density of 1000 deviation scenarios for forecast load demand of 0.35 p.u.

demand follows the mean profile with a standard deviation (SD) of 5% [29]. Taking into consideration the variable consumption patterns, 1000 scenarios of 24 h profiles for single residential or commercial load and single FCS have been generated. Fig. 8 shows the probability density (PD) of 1000 deviation scenarios in relation to the forecast load demand of 0.35 p.u. The Latin hypercube sampling method is applied to ensure that every scenario can be clearly distinguished from other scenarios, reducing the computation burden. With each scenario, mismatch can arise between the grid demand seen from the HV/MV substation and grid demand forecast in Fig. 7 (b), which should be mitigated by the load levelling.

Despite power electronics-based loads and resources not being voltage-dependent, previous studies have confirmed with field experiments that a large amount of voltage dependent loads are still present in the power system [23], [30], [31]. The sensitivity coefficient is variable. As demonstrated in recent field trials, the load sensitivity varies in the range 1–2 p.u., meaning that the load varies its power linearly to quadratic with the voltage variation. In order to include some variability due to the stochastic operation of loads in the distribution grid [18]–[21], [31], the sensitivity coefficients for residential and commercial load types are selected within the following range:

- Residential load: k_{pr} (0.5–2.0); k_{qr} (2.0–3.5)
- Commercial load: k_{pc} (0.5–2.0); k_{qc} (1.0–2.5)

1000 groups of sensitivity coefficients have been developed. The values of sensitivity in each group are randomly selected within the range above. It is noted that low sensitivity coefficients, such as k_p is only 0.5, are also included in the evaluation, ensuring the generality of the analysis. Each group has a significant difference to others thanks to the Latin hypercube sampling method. The 1000 scenarios are evaluated by means of the Monte-Carlo analysis.

The FCS uses the power electronics converter as interface to the AC grid. Consequently, the grid is decoupled from the EV charging facilities inside the FCS. The proposed load levelling approach regulates the voltage of the AC grid within the operation constraints. It is expected that only a few percent of AC voltage variation can be introduced within a time frame of over tens of seconds. As a consequence, the effect on the DC voltage from the AC voltage variation can be neglected. The FCS is considered as constant power load and not sensitive to AC voltage variations.

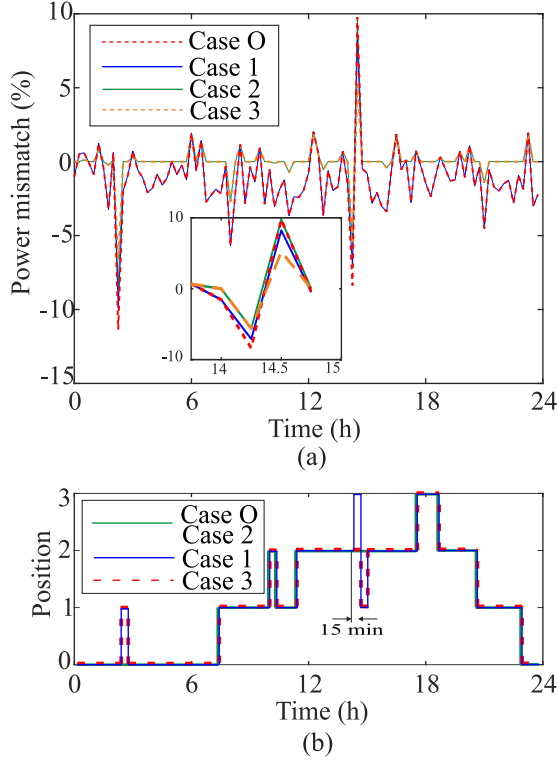


Fig. 9. 24h demand power mismatch and OLTC positions of the time dependent scenario. (a) Power mismatch with respect to the grid demand forecast. (b) Switch of OLTC positions.

TABLE II
SUMMARY OF ACTIVATED ACTUATORS IN EACH CASE

Case	FCSs	OLTC
O	-	-
1	-	✓
2	✓	-
3	✓	✓

B. Test cases and constraints

A common grid condition, suggested by the German distribution system operator, is applied that the SCC is 400 p.u. In order to include all possible grid conditions, different cases for analysis have been defined to include different control actuators. Case O represents the case without any load levelling. It is used as the benchmark to compare the performance of other cases. In case 1, only the OLTC shown in Fig. 6 is used as the actuator. In case 2, the FCSs distributed in different feeders are involved in the load levelling, but the control center does not activate the OLTC, allowing it to be operated under a local voltage control (i.e. $a = 0$). Case 3 denotes the condition, in which the complete load levelling approach with FCSs and OLTC is implemented. A summary of control actuators in the above mentioned cases is listed in Table II.

The values of constraints for the optimization algorithm, including the maximum and minimum voltage and power factor, are listed as follows:

$$V_{\min} = 0.9 \text{ p.u.} \quad V_{\max} = 1.1 \text{ p.u.} \quad \cos\varphi_{\text{sub},\min} = 0.9 \quad (17)$$

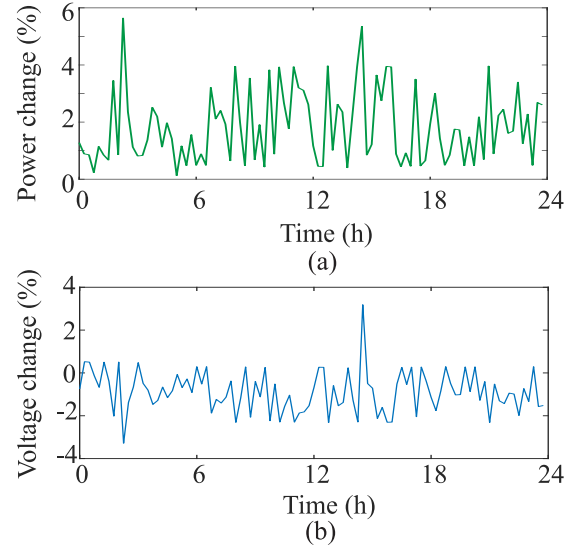


Fig. 10. 24h power and voltage behaviors of last bus in feeder 8. (a) Power change with respect to power without load levelling. (b) Voltage change with respect to voltage without load levelling.

V. ANALYSIS AND DISCUSSION OF RESULTS

This section describes the results obtained by means of the Monte-Carlo analysis, where the aforementioned four cases with 1000 scenarios have been simulated in the MV grid model.

Fig. 9 (a) plots the power mismatch related to the grid demand forecast $P_{\text{grid}}^*(t)$ shown in Fig. 7 (b) in percentage. It is from one of the 1000 time dependent scenarios for Monte-Carlo analysis. The results show that the mismatch in case 1 has no significant difference with respect to case O, i.e., original mismatch; in cases 2 and 3, on average, the power mismatch can be fully compensated, if it in case O is within the 2–3 % range. However, differences rise if the mismatch is higher than 8 %, as can be noted in the time-window 14–16 h. Case 3, with a coordinated action of FCSs and OLTC, is able to further reduce the mismatch with respect to case 2. This time-dependent scenario demonstrates the effectiveness of the proposed load levelling approach, which exploits both the fast dynamics of the load control proposed in [16] and the CVR performance.

The impact of the proposed approach on the OLTC tap is shown in Fig. 9 (b). In cases O and 2, the OLTC is regulated by the local controller, but not considering the load levelling, limiting daily switching at 8 times. If the OLTC is involved in the load levelling, the tapping increases to 14 and 12 times in case 1 and 3, respectively. This is a modest increment of the OLTC switching, which has only limited impact on its lifetime.

With the aforementioned scenario, Fig. 10 shows the change of the load and voltage of the last bus in feeder 8 in Fig. 6. The power change with respect to the power without load levelling in percentage is plotted in Fig. 10 (a). It can be observed that the change within 4 % has a confidence interval of 98 %. Fig. 10 (b) shows voltage change with the voltage without load levelling in percentage. Within a confidence

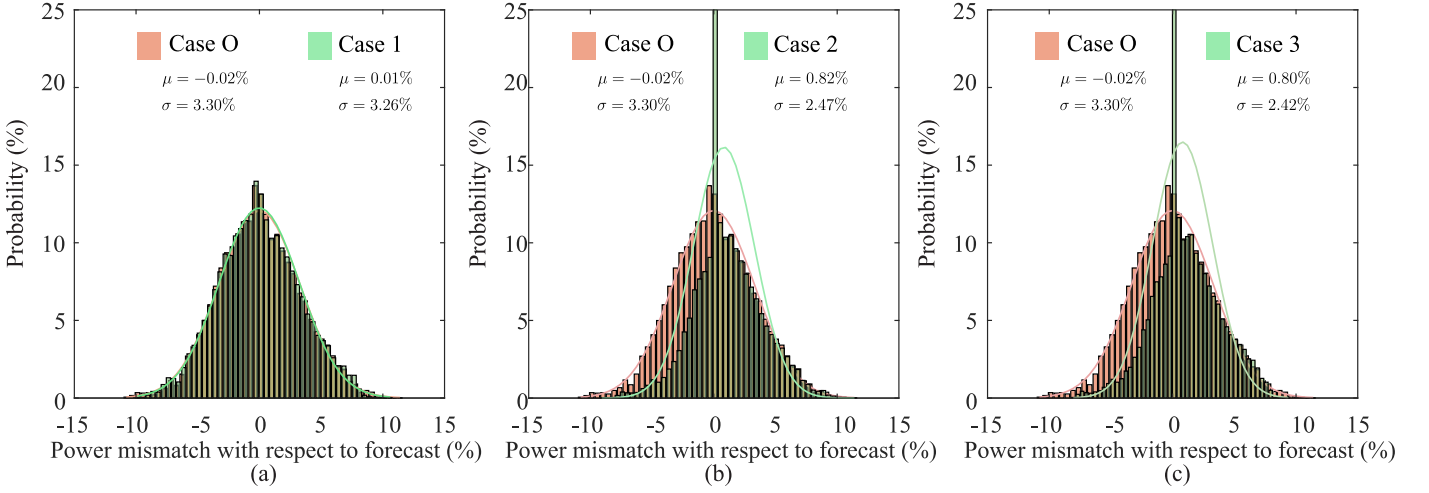


Fig. 11. Probability density of power mismatch in relation to demand forecast $P_{\text{grid}}^*(t)$ in 1000 Monte-Carlo scenarios. (a) Case O vs. Case 1 (with only OLTC). (b) Case O vs. Case 2 (with only FCSs). (c) Case O vs. Case 3 (with both OLTC and FCSs).

interval of 84 %, the voltage variations are within $\pm 0.02\%$. This range of voltage variation has been illustrated by the CVR application in different countries that the quality of power supply to the residential and commercial users is not negatively affected. Furthermore, the voltage constraints are imposed in the algorithm. As a consequence, the voltage of the entire network is controlled within the permitted operation range.

To further investigate the load levelling capability, the power mismatch with respect to the grid demand forecast $P_{\text{grid}}^*(t)$ shown in Fig. 7 (b) is computed. The PD of those results in all scenarios and their corresponding estimated normal distributions are presented in Fig. 11. As can be observed in case 2 and case 3, the probability, when mismatch has large percentage, is significantly reduced. Meanwhile, the probability, when mismatch is around to 0, reaches over 25 % with respect to the case O. The difference between case O and case 1 is small.

Fitting the results into Gaussian Distribution, the standard deviation (SD) of case O is 3.30 %. Summarized in Table III, the value is reduced to 3.26 % with the OLTC (case 1), 2.47 % with the reactive power from FCSs (case 2), and is further reduced to 2.42 % of case 3, respectively. The relative variations of SD with respect to benchmark (case O) $\sigma_x/\sigma_O \cdot 100\%$ (x represents O, 1, 2, and 3) are listed in Table III, in which the SD is reduced by 25 % and 27 % in case 2 and case 3, respectively. The average switching actions in a day of 1000 scenarios is 11.80 times in case O and case 2. The actions in case 1 and case 3 are 13.46 and 12.67, respectively. With the additional actions of the OLTC, the SD in case 3 is decreased by 1.5 % in respect to case 2.

The cumulative distribution (CD) of absolute power mismatch $|P_{\text{grid}}(t) - P_{\text{grid}}^*(t)|/P_{\text{grid}}^*(t)$ in all scenarios is plotted and presented in Fig. 12. It is noted that the curves of case O and case 1 have no significant difference, and the curves of case 2 and case 3 have no significant difference either. However, comparing the curves of case O and case 3, it can be observed that the probability of no mismatch in case 3 reaches 20 %, which is doubled to the probability of no mismatch in

TABLE III
SUMMARY OF MEAN VALUE AND SD OF POWER MISMATCH DERIVED FROM MONTE-CARLO ANALYSIS

Case No.	Mean μ (%)	SD σ (%)	SD with respect to case O (%)	OLTC actions per day
O	-0.02	3.30	100%	11.80
1	0.01	3.26	98.8%	13.46
2	0.82	2.47	74.8%	11.80
3	0.80	2.42	73.3%	12.67

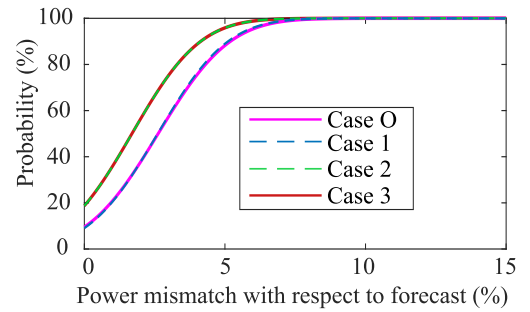


Fig. 12. Cumulative distribution of the absolute power mismatch in 1000 Monte-Carlo scenarios for all cases.

case O. Fig. 13 shows the PD of the absolute power mismatch for case O and case 3. By means of the load levelling approach, the probability, when power mismatch is more than 0.5 %, is reduced significantly.

Fig. 14 shows the reactive power of all 8 FCSs at 9 h 15 min with scenario No.37 of case 3. Stage 1 requires the FCS in feeder 5 to inject more than 0.3 p.u. inductive reactive power and the FCSs in other feeders to inject capacitive reactive power. Stage 2 optimizes the reactive power of all FCSs. The FCSs in feeder 1-3 inject a small amount of inductive reactive power and the injection of capacitive reactive power in feeder 8 is significantly increased. The original grid losses without the load levelling is 0.233 p.u., the losses after implementing the stage 1 and after stage 2 are 0.232 p.u. and 0.230 p.u.,

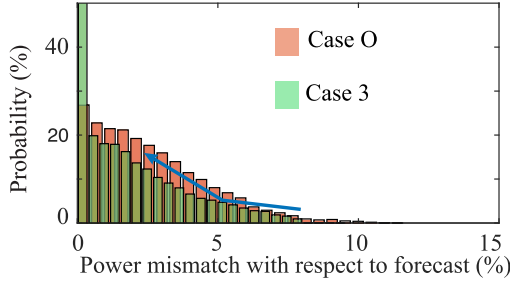


Fig. 13. Probability density of the absolute power mismatch in 1000 Monte-Carlo scenarios for case O and case 3.

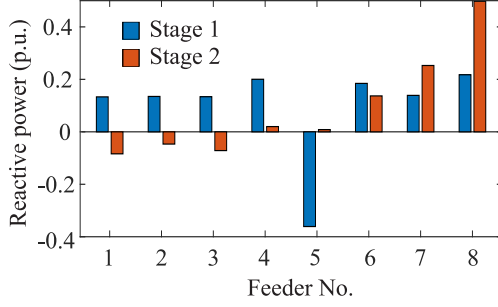


Fig. 14. Reactive power of FCSs, comparison of results of stage 1 and stage 2 in case 3 at 9h 15min with scenario No. 37.

respectively. After stage 2, the losses are reduced by 0.86 %, compared to the losses after stage 1.

The grid losses for case 3 compared to the grid losses for case 1 are evaluated. Fig. 15 (a) shows the PD of losses in all scenarios for case 1 and for stage 1 of case 3. Among 1000 scenarios, in case 1, the probability, if the losses are less than 0.04 p.u., is 18.6 %. The probability is reduced to 12.7 % among the same scenarios in stage 1 of case 3. This implies that the load levelling causes an increase of losses. Fig. 15 (b) shows the PD of losses for case 1 and for stage 2 of case 3. It is observed that among 1000 scenarios, in stage 2 of case 3, the probability is 15.2 %, when the losses are less than 0.04 p.u. The increased losses caused by stage 1 has been improved by stage 2.

The PD of grid power factor in all scenarios, seen from the HV/MV substation, is depicted in Fig. 16. It shows that for case 3, the power factor can be improved with some scenarios and reduced with other scenarios. The improvement of the power factor is due to the injection of capacitive reactive power. The power factor is mostly caused by the injection of inductive reactive power. However, the power factor constraint of 0.9 is never violated.

VI. EXPERIMENTAL DEMONSTRATION WITH POWER-HARDWARE-IN-THE-LOOP TEST

To validate the feasibility and practicality of the proposed approach with realistic grid conditions, an experimental demonstration has been implemented by means of a PHIL system. The PHIL, coupling the hardware under test with a realtime simulated grid, enables to analyze the interaction of the FCS hardware with a realistic grid without the need to realize physically the grid in the laboratory. The configuration

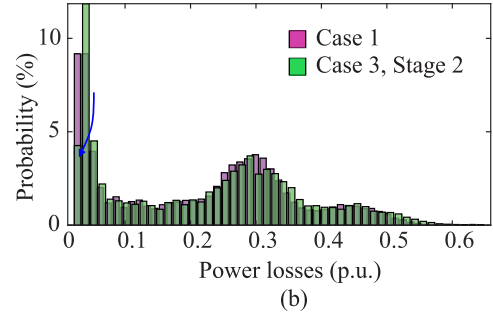
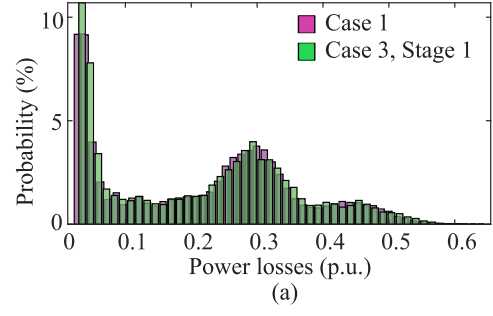


Fig. 15. Probability density of losses in 1000 Monte-Carlo scenarios for case 1 and case 3. (a) Losses in case 1 vs. Losses in stage 1 of case 3. (b) Losses in case 1 vs. Losses in stage 2 of case 3.

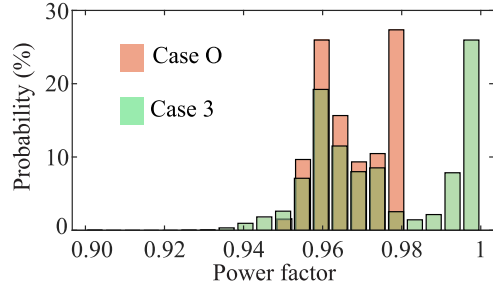


Fig. 16. Probability density of the power factor in 1000 Monte-Carlo scenarios for case 1 and case 3.

of the setup is shown in Fig. 17. The network of the grid is realized in RSCAD, the software of the Digital Real Time Simulator (DRTS), to emulate the grid behavior under the reactive power injection from the FCS. The FCS in RSCAD is modeled as a voltage source with the voltage reference provided by the terminal voltage of the FCS v_{FCS} , i.e. voltage of the hardware. A simulated ideal transformer is used to step up the hardware voltage to the MV level of the grid. A Danfoss FC-302 converter represents the FCS hardware. This converter is indirectly connected to the grid in RSCAD by means of a linear power amplifier (PA) Spitzenberger Spies PAS15000. The active power and reactive power consumption of the converter is determined by the load P_{EV} and the reference Q_{FCS}^* , respectively. A bidirectional DC power supply is used to emulate the charging load P_{EV} . The current in the RSCAD i_{grid} is sampled and sent to the PA controller to reproduce accurately the grid current, testing the impact on the hardware from the grid. A scale factor of 137.5 is introduced between the hardware power and RSCAD to cope with the limited power capability of the converter in the laboratory. The summary of the setup parameters is listed in Table IV.

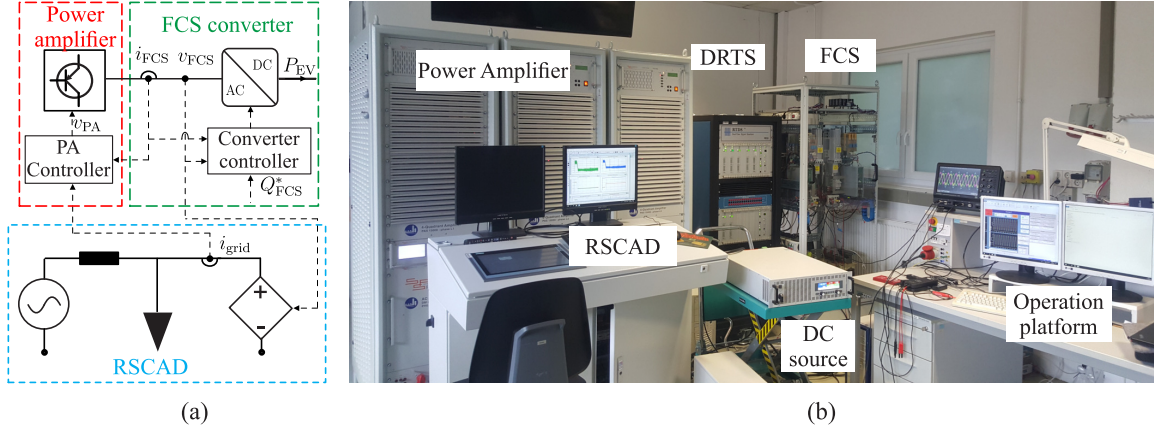


Fig. 17. Laboratory implementation of PHIL. (a) Schematic presentation of PHIL setup. (b) PHIL setup in laboratory.

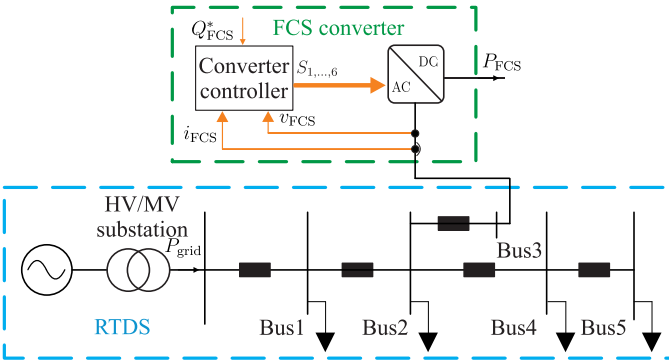


Fig. 18. Schematic representation of the selected feeder 4 in Fig. 6 for the PHIL testing.

TABLE IV
SUMMARY OF PARAMETERS OF PHIL SETUP

Hardware	Parameter	Component in RSCAD	Parameter
PA power rating	15 kVA	Power scaling factor	137.5
Converter power rating	4 kVA	FCS power rating	550 kVA
DC power supply rating	15 kVA		

Feeder 4 of the MV network, as shown in Fig. 6, is selected and simulated in RSCAD. A schematic presentation of the PHIL test network is shown in Fig. 18. Two sets of experiments with both short and long time scale are implemented.

A. Testing of the load levelling approach concept

As first experiment, the performance of the voltage-dependent load levelling approach is demonstrated in a simplified test case. As shown in Fig. 19, the FCS receives the input to inject 0.3 p.u. of inductive reactive power, targeting a reduction of the load power consumption. Starting from 1.5 s, the voltage of bus 4 drops from 0.962 p.u. to 0.946 p.u. (Fig. 19 (b)), with a consequent decrease of the load consumption by 3 % (Fig. 19 (c)). The total feeder power consumption that includes the contribution from the FCS, drops from 2.54 p.u. to 2.48 p.u., obtaining an overall 2.4 % power variation.

As second test, the FCS receives the input to inject 0.3 p.u. of capacitive reactive power with the goal to increase the active power consumption of voltage-dependent loads, as shown in Fig. 20. Starting from 1.5 s, as it can be seen in Fig. 20 (b), the voltage of bus 4 increases from 0.962 p.u. to 0.975 p.u., with a consequent increase of the load consumption by 3 % (Fig. 20 (c)). The total feeder power consumption that includes the contribution from the FCS, increases from 2.54 p.u. to 2.58 p.u., obtaining an overall 1.6 % power variation.

These two tests have demonstrated the capability of voltage-dependent load levelling approach to regulate the load power consumption, both upwards and downwards. This feature allows a higher controllability of the grid that can be only compared to energy storage systems, without, however, installing any additional hardware.

B. Testing the load levelling approach performance in realistic MV grid conditions

In the second set of PHIL experiments, a 15 min demand forecast of the feeder (red line in Fig. 21 (a)) is defined, which is the target of the load levelling approach. The blue and green lines represent the power of the feeder without and with load levelling approach, respectively.

As can be noted in Fig. 21 (a), the power of the feeder $P''_{grid}(t)$ obtained by applying the load levelling approach is nearer to the demand forecast $P^*_{grid}(t)$, showing a clear improvement with respect to power profile of the feeder without load levelling $P'_{grid}(t)$. This improvement can be seen in more detail in Fig. 21 (b), where the power deviation in relation to the forecast of the feeder is plotted. As can be noted, the maximal deviation is decreased from 0.29 p.u. (appearing at 700 s when the power demand is below the forecast) to 0.21 p.u. (also at 700 s). The maximal mismatch is reduced by 28 %.

Both experimental validations clearly show that the load levelling approach can provide an effective control of the load demand within the 2–3 % range, avoiding a cyclic intervention of other actuators, such as batteries.

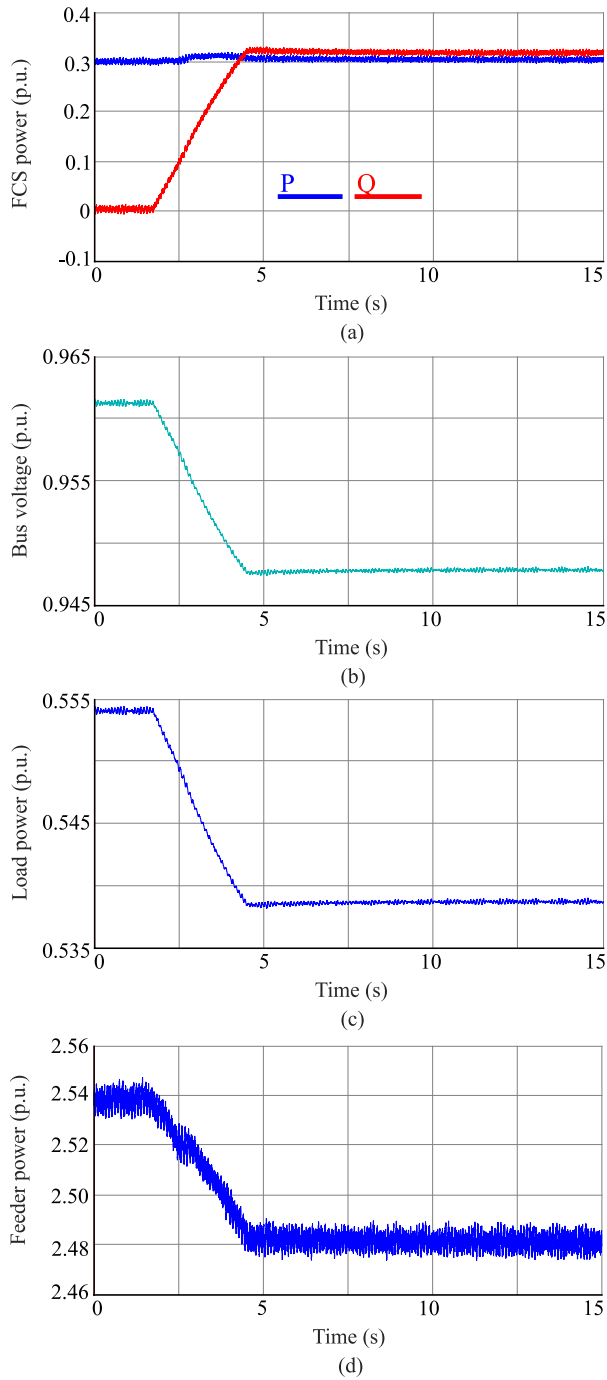


Fig. 19. Voltage and power response to inductive reactive power injection from FCS. (a) Active/reactive power of FCS seen in RSCAD (blue line for active power, red line for reactive power). (b) Voltage response of bus 4 to reactive power injection. (c) Load power of bus 4 to voltage response. (d) Feeder power variation.

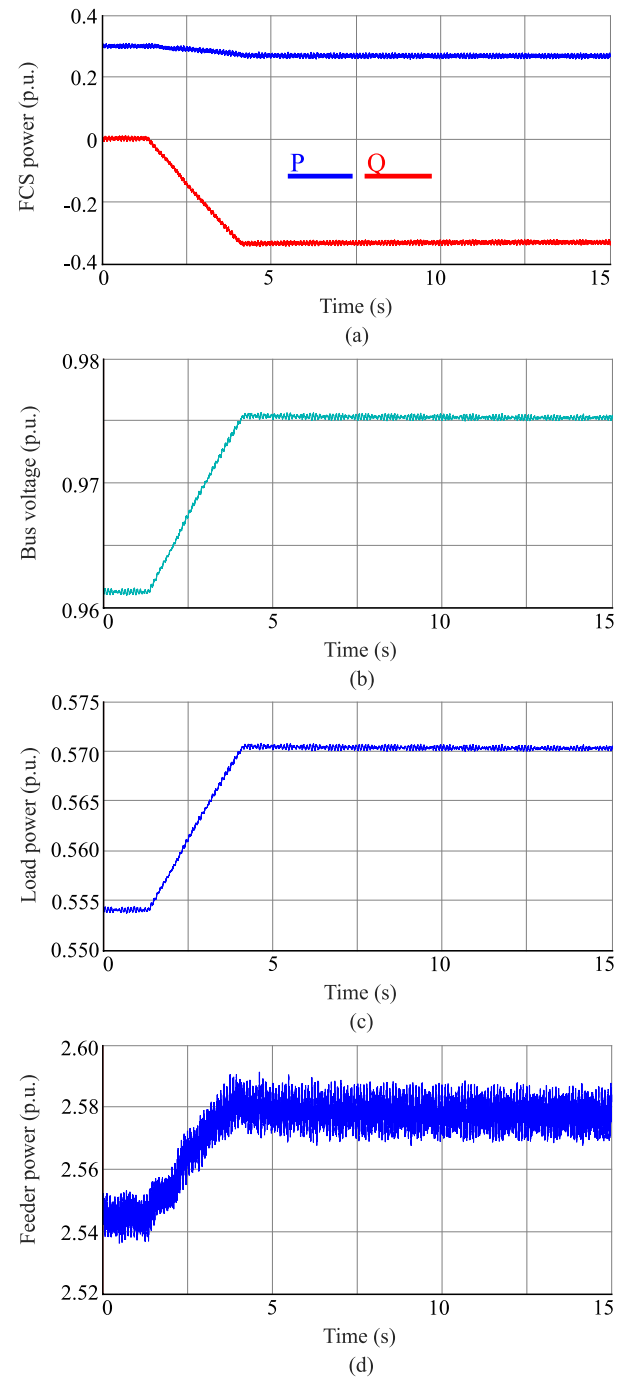


Fig. 20. Voltage and power response to capacitive reactive power injection from FCS. (a) Active/reactive power of FCS seen in RSCAD (blue line for active power, red line for reactive power). (b) Voltage response of bus 4 to reactive power injection. (c) Load behavior of bus 4 to voltage response. (d) Feeder power variation.

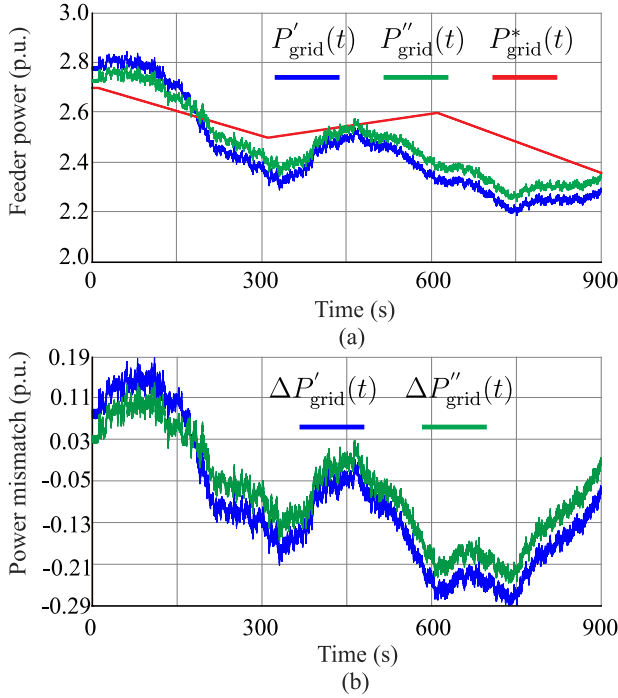


Fig. 21. Performance of load leveling in a 15 minutes time window for the feeder shown in Fig. 18 (red line for demand forecast, blue line for power without load leveling, and green line for power with load leveling). (a) Load power with respect to the demand forecast of the feeder. (b) Power mismatch in relation to the demand forecast of the feeder.

VII. CONCLUSION

A two-stage centralized approach to level the power mismatch between the demand forecast and the realtime demand in MV grids by means of fast charging stations is proposed in this paper. The load levelling approach exploits the voltage-dependent characteristic of the load by making use of the FCS converter's spare power capacity. The voltage of the grid is regulated with reactive power injection, shaping as a consequence the voltage-dependent loads' power consumption. Combined with classical methods, such as OLTC conservation voltage reduction, the proposed approach has been proven effectively in terms of load levelling in a complex MV distribution grid. A Monte Carlo analysis has been performed to represent several grid conditions, including the statistical deviations of power consumption and load sensitivity, in order to generalize the effectiveness of the load levelling approach. With only the OLTC, despite its negligible impact on the losses and power factor, the power mismatch in form of standard deviation can vary only up to 2%. Using only the FCSs, the load levelling approach is able to reduce the mismatch at least of 25%. If a FCSs and OLTC combined control is considered, the power mismatch reduction reaches more than 27%. The second stage of the proposed approach is able to contain the additional losses that are introduced by the first stage of the approach. The results show that the probability of having losses smaller than 0.04 p.u. increases from 12.7% to 15.2% in the second stage with respect to the first one. To demonstrate the effectiveness of the approach in realistic conditions, two power hardware in the loop validations have been performed,

in a short (15 seconds) and a long (15 minutes) time windows. The experimental results confirm the potential of the load levelling approach to level the power consumption in realtime without the need for additional hardware.

REFERENCES

- [1] F. Elghitani and E. El-Saadany, "Smoothing net load demand variations using residential demand management," *IEEE Transactions on Industrial Informatics*, vol. 15, no. 1, pp. 390–398, 2019.
- [2] Q. Jiang, Y. Gong, and H. Wang, "A battery energy storage system dual-layer control strategy for mitigating wind farm fluctuations," *IEEE Transactions on Power Systems*, vol. 28, no. 3, pp. 3263–3273, Aug 2013.
- [3] Y. Li, M. Vilathgamuwa, S. S. Choi, B. Xiong, J. Tang, Y. Su, and Y. Wang, "Design of minimum cost degradation-conscious lithium-ion battery energy storage system to achieve renewable power dispatchability," *Applied Energy*, vol. 260, p. 114282, 2020.
- [4] X. Li, D. Hui, and X. Lai, "Battery energy storage station (bess)-based smoothing control of photovoltaic (pv) and wind power generation fluctuations," *IEEE Transactions on Sustainable Energy*, vol. 4, no. 2, pp. 464–473, April 2013.
- [5] X. Gao, F. Sossan, K. Christakou, M. Paolone, and M. Liserre, "Concurrent voltage control and dispatch of active distribution networks by means of smart transformer and storage," *IEEE Transactions on Industrial Electronics*, vol. 65, no. 8, pp. 6657–6666, Aug 2018.
- [6] L. K. Gan, J. K. H. Shek, and M. A. Mueller, "Analysis of tower shadow effects on battery lifetime in standalone hybrid wind-diesel-battery systems," *IEEE Transactions on Industrial Electronics*, vol. 64, no. 8, pp. 6234–6244, Aug 2017.
- [7] Y. Lin, P. Barooah, and J. L. Mathieu, "Ancillary services through demand scheduling and control of commercial buildings," *IEEE Transactions on Power Systems*, vol. 32, no. 1, pp. 186–197, Jan 2017.
- [8] S. P. Meyn, P. Barooah, A. Busic, Y. Chen, and J. Ehren, "Ancillary service to the grid using intelligent deferrable loads," *IEEE Transactions on Automatic Control*, vol. 60, no. 11, pp. 2847–2862, 2015.
- [9] S. Negarestani, M. Fotuhi-Firuzabad, M. Rastegar, and A. Rajabi-Ghahnavieh, "Optimal sizing of storage system in a fast charging station for plug-in hybrid electric vehicles," *IEEE Transactions on Transportation Electrification*, vol. 2, no. 4, pp. 443–453, Dec 2016.
- [10] Y. Liao and C. Lu, "Dispatch of ev charging station energy resources for sustainable mobility," *IEEE Transactions on Transportation Electrification*, vol. 1, no. 1, pp. 86–93, June 2015.
- [11] J. Hu, C. Si, M. Lind, and R. Yu, "Preventing distribution grid congestion by integrating indirect control in a hierarchical electric vehicles management system," *IEEE Transactions on Transportation Electrification*, vol. 2, no. 3, pp. 290–299, Sep. 2016.
- [12] K. Knezovic, S. Martinenas, P. B. Andersen, A. Zecchino, and M. Marinelli, "Enhancing the role of electric vehicles in the power grid: Field validation of multiple ancillary services," *IEEE Transactions on Transportation Electrification*, vol. 3, no. 1, pp. 201–209, March 2017.
- [13] D. Zhang, L. Y. Wang, J. Jiang, and W. Zhang, "Load prediction and distributed optimal control of on-board battery systems for dual-source trolleybuses," *IEEE Transactions on Transportation Electrification*, vol. 3, no. 1, pp. 284–296, 2017.
- [14] A. Malhotra, G. Binetti, A. Davoudi, and I. D. Schizas, "Distributed power profile tracking for heterogeneous charging of electric vehicles," *IEEE Transactions on Smart Grid*, vol. 8, no. 5, pp. 2090–2099, Sep. 2017.
- [15] H. Zhang, S. J. Moura, Z. Hu, W. Qi, and Y. Song, "Joint pev charging network and distributed pv generation planning based on accelerated generalized benders decomposition," *IEEE Transactions on Transportation Electrification*, vol. 4, no. 3, pp. 789–803, Sep. 2018.
- [16] G. D. Carne, M. Liserre, and C. Vournas, "On-line load sensitivity identification in lv distribution grids," *IEEE Transactions on Power Systems*, vol. 32, no. 2, pp. 1570–1571, March 2017.
- [17] G. De Carne, G. Buticchi, M. Liserre, and C. Vournas, "Load control using sensitivity identification by means of smart transformer," *IEEE Transactions on Smart Grid*, vol. 9, no. 4, pp. 2606–2615, 2018.
- [18] L. M. Korunovic, J. V. Milanovic, S. Z. Djokic, K. Yamashita, S. M. Villanueva, and S. Sterpu, "Recommended parameter values and ranges of most frequently used static load models," *IEEE Transactions on Power Systems*, vol. 33, no. 6, pp. 5923–5934, 2018.

- [19] D. P. Stojanovic, L. M. Korunovic, and J. Milanovic, "Dynamic load modelling based on measurements in medium voltage distribution network," *Electric Power Systems Research*, vol. 78, no. 2, pp. 228 – 238, 2008.
- [20] M. Farrokhhabadi, C. A. Canizares, and K. Bhattacharya, "Frequency control in isolated/islanded microgrids through voltage regulation," *IEEE Transactions on Smart Grid*, vol. 8, no. 3, pp. 1185–1194, May 2017.
- [21] Y. Wan, M. A. A. Murad, M. Liu, and F. Milano, "Voltage frequency control using svc devices coupled with voltage dependent loads," *IEEE Transactions on Power Systems*, vol. 34, no. 2, pp. 1589–1597, 2019.
- [22] X. Gao, G. De Carne, M. Langwasser, and M. Liserre, "Online load control in medium voltage grid by means of reactive power modification of fast charging station," in *2019 IEEE Milan PowerTech*, 2019.
- [23] A. Ballanti and L. F. Ochoa, "Voltage-led load management in whole distribution networks," *IEEE Transactions on Power Systems*, vol. 33, no. 2, pp. 1544–1554, March 2018.
- [24] Z. Wang and J. Wang, "Review on implementation and assessment of conservation voltage reduction," *IEEE Transactions on Power Systems*, vol. 29, no. 3, pp. 1306–1315, 2014.
- [25] L. Calearo, A. Thingvad, K. Suzuki, and M. Marinelli, "Grid loading due to ev charging profiles based on pseudo-real driving pattern and user behavior," *IEEE Transactions on Transportation Electrification*, vol. 5, no. 3, pp. 683–694, 2019.
- [26] A. Ashtari, E. Bibeau, S. Shahidinejad, and T. Molinski, "Pev charging profile prediction and analysis based on vehicle usage data," *IEEE Transactions on Smart Grid*, vol. 3, no. 1, pp. 341–350, 2012.
- [27] G. Hilton, M. Kiaee, T. Bryden, B. Dimitrov, A. Cruden, and A. Mortimer, "A stochastic method for prediction of the power demand at high rate ev chargers," *IEEE Transactions on Transportation Electrification*, vol. 4, no. 3, pp. 744–756, 2018.
- [28] F. Ahmad, M. S. Alam, S. M. Shariff, and M. Krishnamurthy, "A cost-efficient approach to ev charging station integrated community microgrid: A case study of indian power market," *IEEE Transactions on Transportation Electrification*, vol. 5, no. 1, pp. 200–214, 2019.
- [29] R. Bo and F. Li, "Probabilistic lmp forecasting considering load uncertainty," *IEEE Transactions on Power Systems*, vol. 24, no. 3, pp. 1279–1289, Aug 2009.
- [30] A. Ballanti, L. N. Ochoa, K. Bailey, and S. Cox, "Unlocking new sources of flexibility: Class: The world's largest voltage-led load-management project," *IEEE Power and Energy Magazine*, vol. 15, no. 3, pp. 52–63, 2017.
- [31] A. Bokhari, A. Alkan, R. Dogan, M. Diaz-Aguilo, F. de Leon, D. Czarkowski, Z. Zabar, L. Birenbaum, A. Noel, and R. E. Usef, "Experimental determination of the zip coefficients for modern residential, commercial, and industrial loads," *IEEE Transactions on Power Delivery*, vol. 29, no. 3, pp. 1372–1381, June 2014.